High-Temperature Polymorphism in Metastable $BiMnO_3$

Erica Montanari,*,‡ Gianluca Calestani,‡,§ Andrea Migliori,† Monica Dapiaggi,|| Fulvio Bolzoni,§ Riccardo Cabassi,§ and Edmondo Gilioli§

Dipartimento di Chimica Generale ed Inorganica, Chimica Analitica, Chimica Fisica (GIAF), Università di Parma, Parco Area delle Scienze 17A, I-43100 Parma, Italy, CNR-IMM, Area della Ricerca di Bologna, Via Gobetti 101, I-40126 Bologna, Italy, Dipartimento Scienze della Terra, Università di Milano, Via Botticelli 23, I-20133 Milano, Italy, and CNR-IMEM, Parco Area delle Scienze 37/A, I-43010 Parma, Italy

Received July 19, 2005. Revised Manuscript Received September 30, 2005

The multiferroic perovskite $BiMnO_3$, synthesized under high-pressure conditions, decomposes if heated at room-pressure in the temperature range of 500−650 °C. Comparative studies by high-temperature X-ray diffraction, electron diffraction, thermal analysis, and magnetic investigation revealed the existence of a complex pathway to decomposition, depending on the heating rate, pressure, and atmosphere that involves different metastable phases. In particular the as-prepared monoclinic phase (I) transforms to a second monoclinic form (II) at 210 °C and then to an orthorhombic phase (III) at 490 °C. These phase transitions, fast and reversible, occur on heating with a drop in volume and are moved at higher temperatures when pressure is decreased. The transition from II to III, typically observed in inert atmosphere, can be detected also in air when the heating rate is kept sufficiently high. When III is heated in an oxygen-containing atmosphere a slow irreversible transition to variants IV and then V takes place with kinetics depending on temperature, heating rate, and oxygen partial pressure. Both IV and V are oxidized ferromagnetic phases containing Mn^{4+} characterized by a modulated structure based on fundamental triclinic perovskite cells. Their magnetic behavior shows a strong analogy with thin films of $BiMnO_3$, suggesting for the latter an oxidized nature and for the former a possible multiferroic behavior.

Introduction

Solid-state reactions at high pressure, making available phases impossible to obtain at ambient conditions, where however they can survive in metastable form, have recently gained an increased interest. The world of new metastable compounds is wide and fascinating and includes several materials with interesting and attractive properties, such as superconductors and optical materials, as well as super hard materials.[1] The multiferroic bismuth manganite ($BiMnO_3$), a highly distorted perovskite, belongs to such a group of materials. It was synthesized under high pressure for the first time by Sugawara[2] in 1965, and it is a ferroelectric ferromagnet that represents one of the most interesting materials recently studied. In the past few years, studies were devoted to the comprehension of the unusual physical proprieties of $BiMnO_3$: in fact, it is ferromagnetic below 100 K [3] and ferroelectric at room temperature,[4] and promising results for practical applications have been obtained on thin film samples showing large second and third harmonic generation.[5,6] Moreira dos Santos[4] and then Kimura[7] proved the magnetoelectric multiferroic nature of $BiMnO_3$, where ferroelectricity and ferromagnetism coexist below Curie ferromagnetic temperature, leading to a coupling effect at low temperature.

$BiMnO_3$ is usually considered metastable at room pressure, since it cannot be synthesized in this condition by conventional solid-state reactions, giving rise to a mixture of $Bi_2Mn_4O_{10}$ and $Bi_{12}MnO_{20}$. $Bi_2Mn_4O_{10}$ is a mixed valence manganese oxide containing bismuth, presenting orthorhombic symmetry[8,9] and an antiferromagnetic behavior[10] at low temperature (T_N around 40 K), whereas $Bi_{12}MnO_{20}$ is a phase structurally related to δ-Bi_2O_3, from which it can be derived by substituting one Bi atom with a Mn one.[11]

$BiMnO_3$ thin films were grown[12−14] by pulsed laser ablation on perovskite substrate, but, in such cases, it is well-known that the high-pressure requirement for the phase

* Corresponding author. Telephone: +390521905447. Fax: +390521905556. E-mail: erica.montanari@nemo.unipr.it.
‡ Università di Parma.
† CNR-IMM.
|| Università di Milano.
§ CNR-IMEM.

(1) McMillan, P. F. *Nature* **2002**, *1*, 19, and references therein.
(2) Sugawara, F.; Iiida, S. *J. Phys. Soc. Jpn.* **1965**, *20*, 1529.
(3) Sugawara, F.; Iiida, S.; Syono, Y.; Akimoto, S. *J. Phys. Soc. Jpn.* **1968**, *25*, 1553.
(4) Moreira dos Santos, A. F.; Parashar, S.; Raju, A. R.; Zhao, Y. S.; Cheetham, A. K.; Rao, C. N. R. *Solid State Commun.* **2002**, *122*, 49.
(5) Sharan, A.; Lettieri, J.; Jia, Y.; Tian, W.; Pan, X.; Schlom, D. G.; Gopalan, V. *Phys. Rev.* **2004**, *B69*, 214109.
(6) Sharan, A.; An, I.; Chen, C.; Collins, R. W.; Lettieri, J.; Jia, Y.; Schlom, D. G.; Gopalan, V. *Appl. Phys. Lett.* **2003**, *83*, 5169.
(7) Kimura, T.; Kawamoto, S.; Yamada, I.; Azuma, M.; Takano, M.; Tokura, Y. *Phys. Rev.* **2003**, *B67*, 180401(R).
(8) Quezel-Ambrunaz, S.; Bertaut, E. F.; Buisson, G. *C. R. Hebd. Seances Acad. Sci.* **1964**, *258*, 3025.
(9) Bertaut, E. F.; Buisson, G.; Quezel-Ambrunaz, S.; Quezel, G. *Solid State Commun.* **1967**, *5*, 25.
(10) Buisson, G. *Phys. Status Solidi A* **1973**, *16*, 533.
(11) Delicat, U.; Radaev, S. F.; Trömel, M.; Behrens, P.; Kargin, Y. F.; Mar'in, A. A. *J. Solid State Chem.* **1994**, *110*, 66.
(12) Moreira dos Santos, A. F.; Cheetham, A. K.; Tian, W.; Pan, X.; Jia, Y.; Murphy, N. J.; Lettieri, J.; Schlom, D. G. *Appl. Phys. Lett.* **2004**, *84*, 91.
(13) Ohshima, E.; Saya, Y.; Nantoh, M.; Kawai, M. *Solid State Commun.* **2000**, *116*, 73.
(14) Son, J. Y.; Kim, B. G.; Kim, C. H.; Cho, J. H. *Appl. Phys. Lett.* **2004**, *84*, 4971.

10.1021/cm051576w CCC: $30.25
Published on Web 11/12/2005

formation can be efficiently replaced by the lattice pressure of the substrate in forcing the epitaxial growth. On the other hand small dendritic crystals of a phase with composition $BiMnO_3$ were reported to grow at ambient pressure, as minority phase, from a melt of composition 80 mol % Bi_2O_3 and 20 mol % Mn_2O_3 by Bokov.[15] These results were partially confirmed by further experiments,[16] in which, by following the indication of Bokov, traces of $BiMnO_3$ were found in polyphasic samples. Since the growth from the melt is driven by crystallization kinetics, the obtainment of a phase in a $P-T$ region, which is outside its thermodynamic stability in the absence of the liquid phase, is not surprising. However the lattice parameters given by Bokov for these $BiMnO_3$ crystals ($a = c = 7.86$ Å, $b = 7.98$ Å, $\alpha = \gamma = 91.67°$, $\beta = 90.97°$) differ from the usually accepted structure, which consists of a fundamental triclinic perovskite cell[3] ($a = c = 3.935$ Å, $b = 3.989$ Å, $\alpha = \gamma = 91.46°$, and $\beta = 90.96°$) showing a monoclinic $C2$ superstructure[17] ($a = 9.54$ Å, $b = 5.61$ Å, $c = 9.86$ Å, and $\beta = 110.7°$). Even if clearly related to the fundamental substructure reported for the high-pressure prepared phase, the data of Bokov lead to a different superstructure ($a = 10.93$ Å, $b = 11.31$ Å, $c = 7.98$ Å, and $\beta = 92.4°$). Due to the complexity of the $BiMnO_3$ structure and to the limited structural characterization at that time performed on these crystals, it is impossible to draw a definitive conclusion on their nature. On one side, the strong analogies in the magnetic behavior suggest the phase grown from melt to be the same prepared at high pressure. On the other side, the observation by electron diffraction (ED) of a second polymorph in samples prepared at high pressure led Chiba et al. to conclude[18] its possible equivalence with the Bokov phase. However, a detailed study[19] recently performed by our group on the existence of polymorphisms at room temperature in $BiMnO_3$ prepared at high pressure, showed the structural features of the second polymorph (present as the minority phase and thereinafter denoted as I*) to be not consistent with this hypothesis, being this phase is characterized by a complex pseudo-rhombohedral superstructure ($a = 13.62$ Å, $b = 13.66$ Å, $c = 13.66$ Å, $\alpha = 110°$, $\beta = 108.8°$, and $\gamma = 108.8°$) and by a magnetic transition at a temperature (107 K) higher than the conventional polymorph (thereinafter denoted as I).

The thermal evolution of $BiMnO_3$ at ambient pressure was studied at first by Faqir in 1999,[20] by means of high-temperature X-ray diffraction analysis (HTXRD), thermal analysis, and magnetic measurements and successively by Kimura[7] in 2003, by using similar techniques. $BiMnO_3$ decomposes, if heated at ordinary pressure above 600 °C, into a mixture of $Bi_2Mn_4O_{10}$ and bismuth oxides. Before decomposition, $BiMnO_3$ undergoes two phase transitions. The first, reversible, occurs at 210 °C and is related to a change of the $C2$ monoclinic superstructure. The second, irreversible, takes place at around 500 °C and leads to a tetragonal phase (according to Faqir et al.[20]) or to an orthorhombic phase (according to Kimura et al.[7]). Thermal analysis and resistivity measurements at the transition temperatures show the first-order nature of both of the structural transitions. No details about the crystal structure of the different forms appearing during the heating process have been reported yet.

Ferroelectric hysteresis loop was observed in both bulk and thin film samples up to about 120 °C,[4] since investigation at higher temperatures are hampered by the low resistivity of the specimens. Despite this in the literature is usually accepted that the ferroelectric Curie temperature could be related to the second structural transition, at least from a crystallographic point of view.[7] Nevertheless, a comprehensive analysis of the thermal behavior of the $BiMnO_3$ in that temperature range is requested in order to clarify all the open questions concerning the real nature of the structural transitions and the relation with the appearing of a paraelectric state.

Therefore, we decided to investigate the thermal evolution of the metastable-phase $BiMnO_3$ up to the decomposition temperature by characterizing it from structural and magnetic point of views. $BiMnO_3$ samples were prepared by solid-state reaction under high-pressure conditions, and then a deep study was carried out by high-temperature X-ray diffraction and thermal analysis. The results are coupled, when possible, with selected area electron diffraction (SAED) and high-resolution electron microscopy (HREM) investigation at room temperature and magnetic measurements at low temperature. The existence of a different thermal pathway depending on the heating rate and conditions is pointed out in this work, revealing a much more complex picture of the $BiMnO_3$ polymorphisms on its way to decomposition.

Experimental Section

Polycrystalline samples of $BiMnO_3$ were synthesized by using a high-pressure multianvil apparatus in the experimental conditions (40 kbar, 450 °C, and 20 h), leading to the minimization of the oxycarbonate impurity.[19] As starting material, a mixture of bismuth oxide (Bi_2O_3, Aldrich 99.99%) and manganese(III) oxide (Mn_2O_3, Aldrich 99.999%) in stoichiometric molar ratio was used. Powder reagents were carefully mixed and ground, pelletized (diameter = 5 mm), encapsulated in a Pt foil (30 μm thick), inserted in an octahedral MgO cell assembly and placed in a 6/8-type multianvil apparatus (Rockland Research Corp.). After the application of desired pressure (increasing rate = 120 bar/min), the sample was heated at the reaction temperature at a rate of 50 °C/min. After reaction the sample was quenched to room temperature (RT), and finally the pressure was slowly released (−50 bar/min). The reaction temperature was monitored by a Pt/Pt−Rh10% thermocouple, in direct contact with the capsule. The prepared sample was characterized by high-temperature X-ray powder diffraction (HTXRPD) in the temperature range from room temperature to 450 °C by using a Thermo ARL X'tra diffractometer, equipped with Cu Kα radiation ($\lambda = 1.541\,78$ Å) and a Thermo Electron solid-state detector. Patterns were also collected up to 550 °C by using a diffractometer Philips Xpert with $\theta-\theta$ geometry, equipped with a hot chamber (PAP1600) with a maximum temperature of 1600 °C, carefully

(15) Bokov, V. A.; Myl'nikova, I. E.; Kizhaev, S. A.; Bryzhina, M. F.; Grigoryan, N. A. *Sov. Phys. Solid State* **1966**, *7*, 2993.
(16) Chiba, H.; Atou, T.; Syono, Y. *J. Solid State Chem.* **1997**, *132*, 139.
(17) Atou, T.; Chiba, H.; Ohoyama, K.; Yamaguchi, Y.; Syono, Y. *J. Solid State Chem.* **1999**, *145*, 639.
(18) Chiba, H.; Atou, T.; Faqir, H.; Kikuchi, M.; Syono, Y.; Murakami, Y.; Shindo, D. *Solid State Ionics* **1998**, *108*, 193.
(19) Montanari, E.; Righi, L.; Calestani, G.; Migliori, A.; Gilioli, E.; Bolzoni, F. *Chem. Mater.* **2005**, *17*, 1765.
(20) Faqir, H.; Chiba, H.; Kikuchi, M.; Syono, Y.; Mansori, M.; Satre, P.; Sebaoun, A. *J. Solid State Chem.* **1999**, *142*, 113.

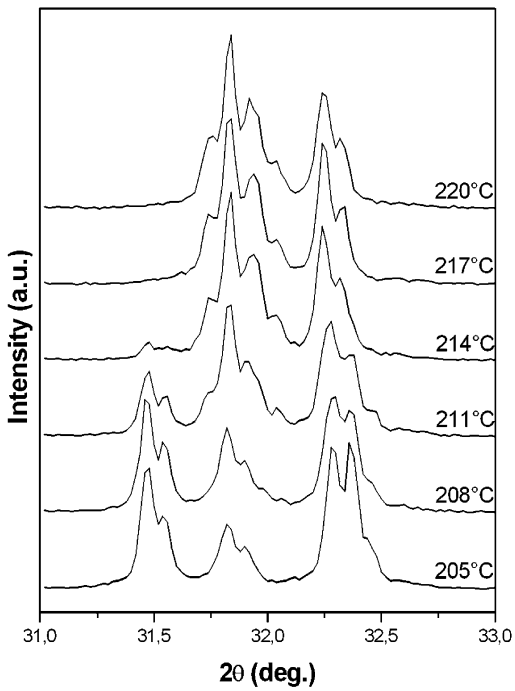

Figure 1. Thermal evolution of a portion of XRPD pattern in the I−II transition region.

calibrated for temperature and sample position. Collecting conditions were typically 0.01−0.02° steps and 5−10 s/step counting times. Structural data were analyzed by Rietveld refinement using the GSAS program.[21]

Transmission electron microscopy (TEM) analyses were performed at room temperature by using Philips Tecnai F20 working at 200 kV. The specimens were prepared by grinding the samples in isopropyl alcohol and by evaporating the suspension on a copper grid covered with a holey carbon film. SAED and HREM images were collected by a Gatan slow-scan CCD camera.

Magnetization curves were measured in both field- cooling (FC) and zero-field-cooling (ZFC) modes in the temperature range of 5−200 K with a superconducting quantum device (SQUID) magnetometer (Quantum Design).

Thermal analyses, in particular differential scanning calorimetry (DSC) and thermogravimetric analysis (TGA), were performed on powder samples, either in air or in nitrogen atmosphere, by using Perkin-Elmer DSC 7 and Perkin-Elmer TGA 7, respectively. The heating rate was varied from 0.5 to 20 °/min.

Results and Discussion

Reversible I−II Transition. According to literature data,[20] a first phase transition of polymorph I to a different monoclinic form (thereinafter denoted by II) was detected at room pressure at 210 °C. Figure 1 shows the thermal evolution, in the transition region, of the multiplet related to the fundamental 110 reflection of the perovskite cell. In this experiment, the warming process was carried on slowly in order to keep a uniform temperature across the sample. The transition displays a thermal hysteresis, whose gap is mainly independent of the experimental conditions and is perfectly reversible on cooling, even if an extremely high cooling rate are used. In fact the quenching in liquid nitrogen of a $BiMnO_3$ specimen, sealed in an Ag capsule and heated for 30 min, well above the transition temperature returned the starting polymorph I.

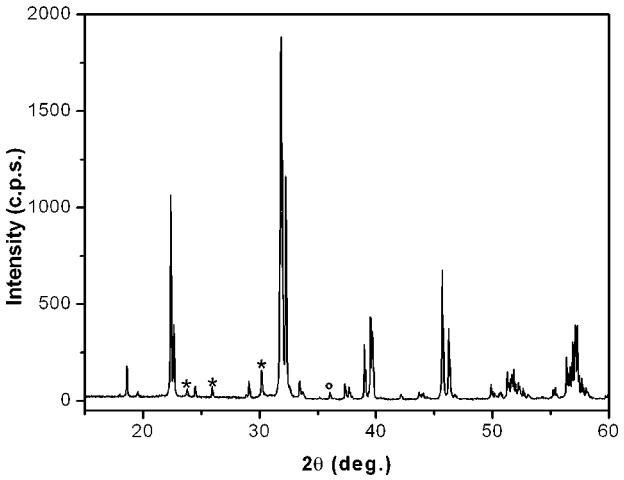

Figure 2. XRPD pattern of polymorph II taken at 225 °C in air. The impurity phases present in the sample are marked: bismuth oxycarbonate (star) and Mn_3O_4 (circle).

This behavior suggests a displacive, rather than reconstructive, character of the phase transition that agrees with the structural features of II. In fact, in comparison with I, the new polymorph shows a slightly distorted cell (a = 9.5421(2) Å, b = 5.6114(1) Å, c = 9.8590(2) Å, β = 110.628(1)° and a = 9.5815(3) Å, b = 5.5973(2) Å, c = 9.7446(4) Å, β = 108.65(1)° for I and II, respectively) and a similar diffraction symmetry (possible space groups from systematic absences are *C*2, *Cm*, or *C*2/*m*). On the basis of the fundamental perovskite cell, II presents a distortion consisting of two equal edges and a shorter one as previously reported[3] ($a = b$ = 3.970 Å, c = 3.924 Å, α = 90.68°, β = 89.32°, γ = 90.39° for the basic triclinic unit cell), opposite to that of the room temperature form I, that presents two equal edges and a longer one ($a = c$ = 3.935 Å, b = 3.989 Å, $\alpha = \gamma$ = 91.46°, and β = 90.96°). When the lattice parameters of the perovskite subunit are taken into account, a strong similarity between polymorphs II and I* could be hypothesized. However, when the complete diffraction pattern is considered, the different nature of the two phases is revealed. The powder diffraction pattern of II is shown in Figure 2.

The observed reversibility of the phase transition agrees with the endothermic effect detected on heating by DSC at the phase transition. Being I at room conditions a metastable phase, the I−II transition should be interpreted thermodynamically as a transformation that occurs in a metastability regime (from a metastable phase to another metastable phase). As shown in Figure 3, where the volume of the fundamental $BiMnO_3$ perovskite cell determined in our experiments (by powder XRD) is plotted vs temperature, both I and II are characterized by a positive thermal expansion, but the transition occurs with a decrease in volume.

If the temperature-dependent diffraction experiment is performed in a vacuum ($P < 10^{-5}$ bar), the I → II transition keeps its typical character but is displaced at higher temperature (about 380 °C), confirming the stabilizing effect of the external pressure on the existence range of polymorph

(21) Larson, A.; von Dreele, R. B. *General Structure Analysis System (GSAS);* Report LAUR 86-748; Los Alamos National Laboratory: Los Alamos, NM, 1994.

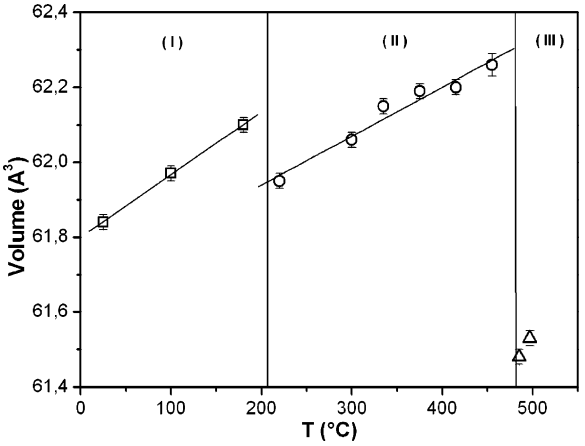

Figure 3. Temperature dependence of the cell volume of $BiMnO_3$ polymorphs in terms of fundamental perovskite sublattice. The evolution through subsequential structural transitions is pointed out: I, from room temperature to 210 °C (squares); II, from 210 to 490 °C (circles); III, from 490 °C (triangles).

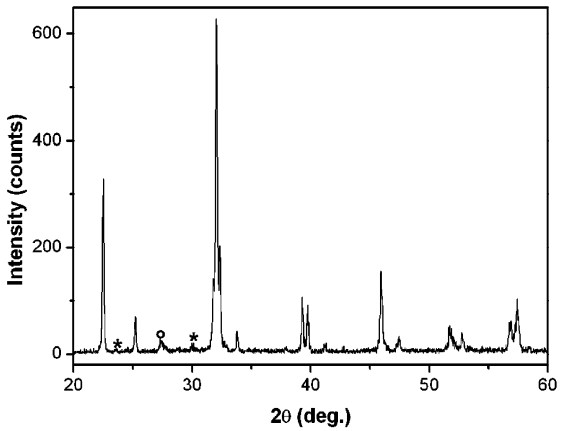

Figure 4. Diffraction pattern of polymorph III recorded at 490 °C in air. The impurity phases present in the sample are marked: bismuth oxycarbonate (stars) and $Bi_{12}MnO_{20}$ (circle). Both impurities have been present in the as-prepared compound and do not change in amount during the phase transition.

II suggested by the decrease of volume associated to the phase transition.

Reversible II−III Transition. When polymorph II is heated at room pressure in a relatively fast way (heating rate $\geq 0.6°$ min^{-1}), a second endothermic phase transition occurs around 490 °C. In these conditions $BiMnO_3$ transforms into an orthorhombic phase (thereinafter denoted by III), whose diffraction pattern (reported in Figure 4) is similar to that of the orthorhombic calcium-doped bismuth manganite $Bi_{1-x}Ca_xMnO_3$.[22] The unit cell of III ($a = 5.537(1)$ Å, $b = 5.629(1)$ Å, $c = 7.897(1)$ Å, $\alpha = \beta = \gamma = 90°$) represents the classical structure of $LnMnO_3$ perovskites (Ln = La, rare earths) and their solid solution with alkaline cations ($a \approx b \approx \sqrt{2}a_P$, $c \approx 2a_P$, where a_P = perovskite edge). From systematic absences, the possible space groups are restricted to *Pbnm* and $Pbn2_1$. As with the first transition, this second one is fast and completely reversible, so that a phase III sample cooled at room-temperature returns the phase I through a III → II → I pathway. Quenching the sample in liquid nitrogen is not able to prevent this transition, suggesting a displacive character for all the transformations. As shown in Figure 3, the II−III transition involves again a decrease in volume of the basic perovskite and the thermodynamic considerations previously made for the I−II transition can be extended to the present case.

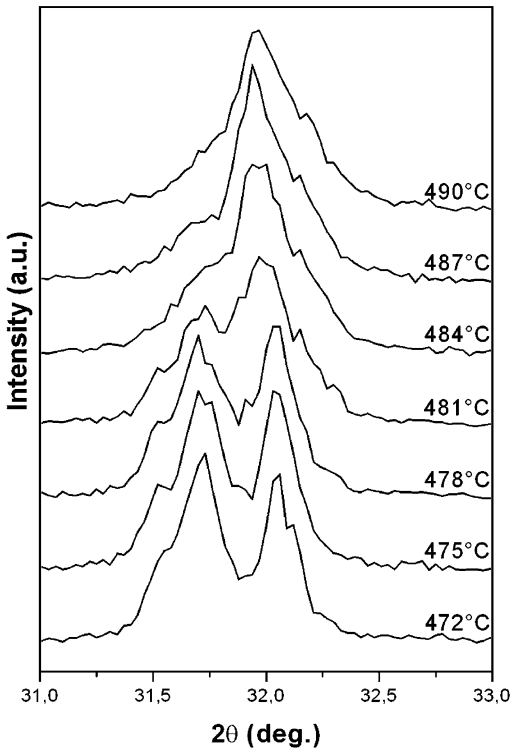

Figure 5. Thermal evolution of a portion of XRPD pattern in the II−IV transition region.

Irreversible Transitions to Forms IV and V. When operating in air, polymorph III is transformed in a new structural variant, thereinafter denoted by IV. That transition, characterized by a considerable slow kinetic, occurs above the II−III transition (490 °C). By isothermal treatment, the requested time for the transformation decreases by increasing the temperature. Otherwise, by increasing the temperature, the critical point strongly depends on the heating kinetics being higher for a faster heating. If the rate is kept below 0.5° min^{-1}, II converts directly to IV at about 490 °C, as shown in Figure 5 by the evolution, in the transition region, of the XRD multiplet related to the fundamental 110 reflection of the perovskite cell.

The transition is irreversible, and phase IV can be recovered at room temperature independently from the cooling rate. The diffraction pattern of the new variant (Figure 6a) is characterized by very broad peaks corresponding to the fundamental perovskite reflections. Due to the peak broadness and to the close *d* values, the completeness of the phase transition cannot be determined by HTXRD experiments. However, since residual III converts in I by cooling, the deconvolution of the diffraction pattern becomes easier at room temperature, permitting one to point out the occurrence of incomplete transformations. The existence of a phase quite similar to IV was previously reported by Faqir,[20] and its diffraction was interpreted in terms of a tetragonal cell. However our data clearly demonstrate the

(22) Bokov, V. A.; Grigoryan, n. A.; Bryzhina, M. F. *Phys. Status Solidi* **1967**, *20*, 745.

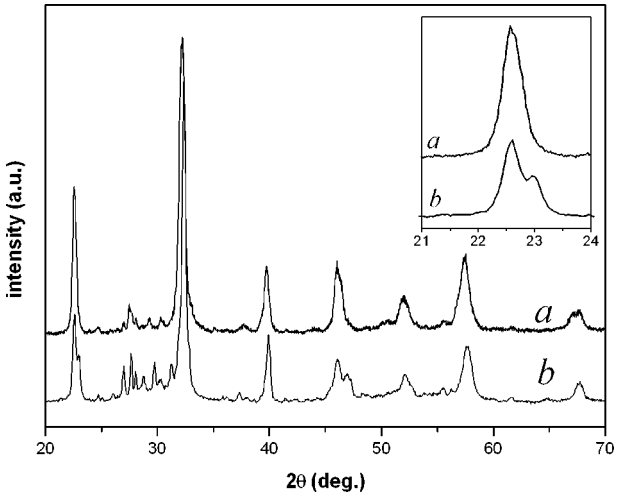

Figure 6. XRD pattern of $BiMnO_3$ samples, recorded in air at room temperature after different thermal treatments: (a) slow heating (0.5°/min.) to 510 °C and quenching to RT; (b) slow heating to 500 °C followed by a 6 h annealing at this temperature and quenching to RT. A detail of the evolution of the 100 fundamental perovskite reflection is shown in the inset. Pattern a can be considered typical of phase IV, whereas b is representative of phase V. The transformations are related to a progressive segregation of impurities phases, in particular Bi_2O_3 and $Bi_{12}MnO_{20}$, whose diffraction peaks are mainly evident in the 26−30° 2θ region.

impossibility of indexing the pattern on a similar basis and suggest the peak broadness to be derived not only from a loss of crystallinity during the phase transition but also from a severe superimposition of unresolved multiplets, such as those expected from a low-symmetry slightly distorted perovskite.

Attempts to reduce the peak broadness by prolonged heating just above the transition temperature failed and resulted in a significant change of the XRD pattern, retained at room temperature (Figure 6b), that can be justified only by considering the formation of a different perovskite phase, thereinafter denoted by V. As shown in the inset of Figure 6, showing the evolution, with the increase of the annealing time, of the fundamental 100 perovskite reflection, the broad peak typical of phase IV resolves into a doublet (or more probably a triplet), indicating that a lattice parameter becomes remarkably shorter than the others. Preliminary attempts to index the XRD patterns led to the exclusion of the existence of high symmetry, suggesting that V could be a further low-symmetry distorted perovskite. As in the previous case, the diffraction pattern is characterized by broad peaks that could be produced by both reduced grain size and superimposition of unresolved multiplets.

XRD patterns taken at room temperature suggest a contraction of the cell volume passing from III to IV to V, as confirmed in the following section by the determination of the lattice parameters, made possible by coupling these results with electron diffraction data. A similar contraction is qualitatively observed also in HTXRD patterns, but the continuous nature of the transitions leads to a change of the diffraction pattern during the collection of reasonable quality data.

In air some hours of isothermal treatment in the range of 490−500 °C convert almost completely III in V (via IV). When the partial pressure of oxygen is reduced, the kinetics of the irreversible transitions to IV decreases until it is inhibited in inert atmosphere (nitrogen or argon). This agrees with the results of Kimura, who obtained phase III by heating $BiMnO_3$ in argon. The need of an oxygen-containing atmosphere to produce IV and V suggests these variants to be "oxidized" forms. The influence of the external atmosphere on these transformations was confirmed by comparative XRD experiments performed at RT on equivalent amounts of powders and ceramic pellets previously heated in the transition region. The results indicated a complete transition for the powdered samples, whereas the pellets were found to include a polymorph I core deriving from the nontransformation of the protected III core at high temperature.

The perovskite is a quite dense structure, for which an oxidized form can be thought in terms of cation deficiency, rather than of extra oxygen. Therefore, the formation of an oxidized form should necessarily be considered a chemical reaction that on one side involves atomic mobility and slow kinetics and on the other side the segregation of secondary phases, features that characterize the formation of IV and V. In particular, as shown in Figure 6, the progressive transformation into IV and V, observed by increasing the annealing time, is related to a progressive segregation of Bi-rich impurities, in agreement with a higher Mn^{4+} content of phase V. We attempted to determine, by performing TGA in air, the variation of composition connected with the transformations, but the weight changes are too small to be reliably determined, in particular by taking into account that the samples are always contaminated by bismuth oxycarbonate, formed during the starting synthesis, whose decomposition can partially mask the weight gain produced by the oxidation.

Being obtained through a chemical reaction involving a change of the chemical composition, phases IV and V cannot be strictly considered $BiMnO_3$ polymorphs. However, they preserve a strong structural analogy with the $BiMnO_3$ phases, of which they can be considered compositional variants.

Thermal Decomposition of the Perovskite. In air above 520 °C, forms IV and V start to decompose with a kinetics that increases by increasing temperature; the decomposition, which becomes fast above 600 °C, leads to the stable-phase $Bi_2Mn_4O_{10}$ with segregation of $Bi_{12}MnO_{20}$ and/or Bi_2O_3 (the reaction products of an equimolar $Bi_2O_3-Mn_2O_3$ mixture at room pressure). In nitrogen, the direct decomposition of III occurs, and, for example, it is observed around 650 °C if the sample is heated at 20° min^{-1}.

Magnetic Characterization. Magnetic measurements, both field-cooling (FC) and zero-field-cooling (ZFC), were performed on $BiMnO_3$ samples as obtained after different thermal treatments. In particular, the magnetic characterizations were carried out on the I form, as prepared and as gained from the complete reversible pathway after the formation of II and III, and on the IV and V forms obtained by the irreversible transformations.

$BiMnO_3$ prepared by high-pressure synthesis consists, as previously observed,[19] of two different polymorphs, I and I*; I is the well-known monoclinic *C*2 form characterized by a ferromagnetic Curie temperature at 99 K, whereas I* is a minority phase with a higher critical magnetic temper-

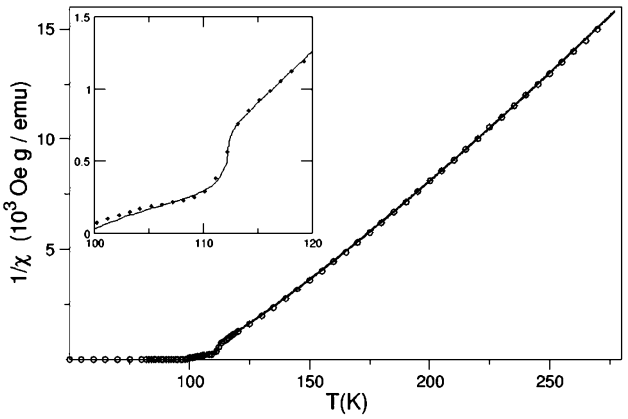

Figure 7. Inverse susceptibility in 10 Oe magnetic field. The line corresponds to the best fit for two ferromagnetic phases with transition temperatures of 99 and 112 K, with a 0.3% of the 112 K phase.

ature. The coexistence of the two phases with different critical temperatures results in a characteristic magnetic response. As shown in Figure 7 the inverse susceptibility vs temperature curve approaches a Curie−Weiss behavior and exhibits a peculiar anomaly near T_C. The anomaly can be explained as the overall magnetic response of two ferromagnetic phases with different transition temperatures. The experimental points are well-fitted by a linear combination of the two phases, assuming that each one follows a classical power law both over and under its own T_C (99 and 112 K). Leaving the linear combination coefficients and the power exponents of each phase as free parameters in the best-fit procedure, and assuming similar Bohr magneton number for the two phases, one can also estimate the percentage contribution of each phase. Several fittings performed on different as-prepared samples show that the amount of I* varies from few per mill to a few percent, depending on the experimental synthetic conditions in agreement with the suggestion of I* as a surface phase.[19] Magnetic investigations carried out on samples obtained at room temperature after thermal treatment, performed in such a way to avoid the formation of IV and V, confirm the preservation of I and the disappearance of I*.

Concerning IV and V, it must be pointed out that the achievement of pure phases is practically impossible, because of the slow kinetics and of the simultaneous occurrenc of different phenomena. Since the oxidation reaction starts from the grain surface and continues toward the interior, V contaminates IV before III disappears completely. The same happens with V that starts to decompose before IV transforms completely. Therefore, we studied some samples, thereinafter denoted by A, B, C, and D, which have undergone different treatments. A and B, a sintered pellet and a powder sample, respectively, have been heated slowly (0.5°/min.) up to 510 °C (I → II → IV); C has been introduced in a furnace preheated at 500 °C (I → II → III**)** and then annealed at this temperature for 12 h (III → IV → V). D has undergone a treatment similar to A and B (I → II → IV), followed by an annealing at 500° for 6 h (IV → V).

The magnetic measurements are in agreement with the comparative study performed by XRD. As shown in Figure 8, the FC behavior of the sintered sample (A) reveals the presence of three magnetic contributions: the onset of the

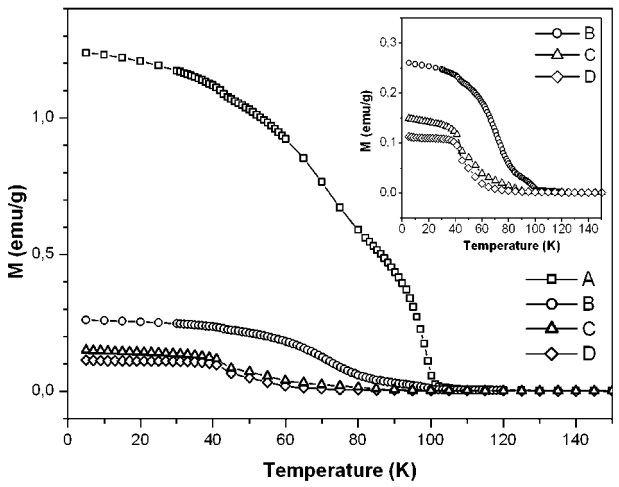

Figure 8. Magnetization vs temperature for $BiMnO_3$ samples A−D. The plots refer to measurements performed by cooling in 10 Oe magnetic field. In the inset, a zoom of the curves for samples B−D at low temperature is shown.

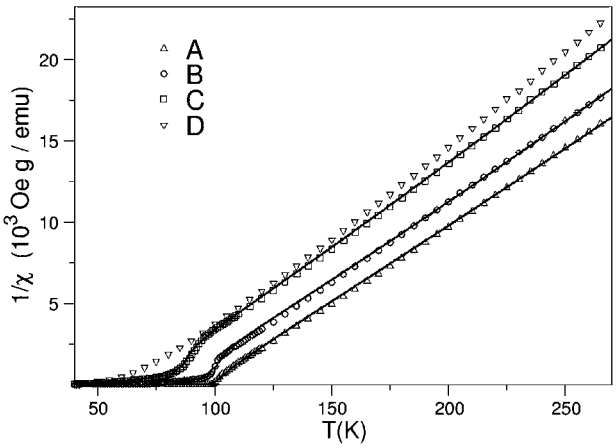

Figure 9. Inverse susceptibility in 10 Oe magnetic field for A−D samples with best fits for two main ferromagnetic phases. The corresponding transition temperatures are 71 and 99 K in A and B, 50 and 85 K in C, and 50 K in D. See text for further details.

characteristic ferromagnetic response of I at 99 K, a broadened transition around 70 K, and a further small anomaly at about 50 K. According to XRD data, showing for this sample the coexistence of I and IV, the transition at 70 K is linked with the formation of IV. The transition is broadened because of the strong inhomogeneities produced by the oxidation of a sintered sample. A nonuniform oxidation leads to a nonuniform distribution in the formation of IV and in a wide magnetic response. The study of the powder sample (B) shows, as expected, that the transition at 70 K becomes dominant and confirms the anomaly at 50 K. As shown in Figure 9 the inverse susceptibility is characterized by anomalies near T_C similar to those previously produced at higher temperatures by the coexistence of the ferromagnetic I and I* phases in as-prepared samples. By taking into account only the main magnetic components, both A and B curves have been modeled with two ferromagnetic phases with T_C fixed at 71 and 99 K. In this case, the model still assumes the same magneton number for the two phases, a hypothesis that can be considered acceptable in first approximation for the partially oxidized IV phase. Within the used approximations the amount of I in the

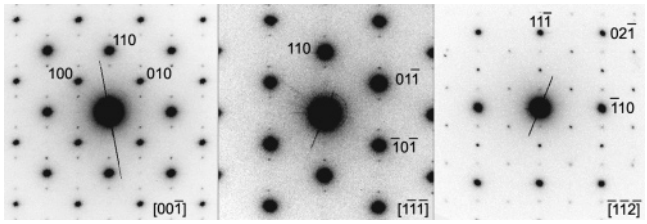

Figure 10. SAED patterns recorded in different zone axes, indexed on the basis of the fundamental perovskite cell, showing the typical satellite spots of phase IV.

sample, estimated by fitting of the inverse susceptibility vs temperature curves, decrease from 47% in A to 2% in B. Although not clearly detectable by XRD (Figure 6a), the presence of residual I is revealed by the magnetic measurement.

The moment at 5 K, strongly depressed in sample B by the decrease of the phase I content, is further on reduced in samples C and D, where the anomaly previously recorded at 50 K becomes the dominant magnetic effect. By comparison with XRD results (Figure 6b), this magnetic effect can be associated to phase V. The transition is very broad in sample C, where a long tail extends at higher temperatures. The fitting of the inverse susceptibility requires an additional magnetic contribution at higher temperature. The situation is satisfactory fitted by taking into account the presence of a small amount (5%) of a further ferromagnetic phase with T_C at about 85 K. On the contrary in sample D the transition becomes sharper and no anomaly can be detected in the inverse susceptibility curve, where just a progressive deviation from the Curie −Weiss law is observed approaching T_C. The differences between C and D samples probably reflect the different synthetic path, involving or not the formation of polymorph III. Once it is formed, III transforms slowly at the annealing temperature into IV, that in its own turn changes gradually in V. Consequently, despite the longer thermal annealing, the transition to V is still incomplete in sample C, whereas for sample D a shorter annealing directly performed on IV results in an almost complete transformation.

TEM Characterization. The $BiMnO_3$ samples used in this work, as prepared and recovered at room temperature after different thermal treatments, were characterized by TEM. Selected area electron diffraction and high-resolution electron microscopy studies were coupled to derive structural information on the different manganites, which can be obtained as metastable phase at room temperature.

According to a previous work (Montanari et al.[19]), the as-prepared samples were found to consist of two different polymorphs, I and I*, the latter mainly segregated at the grain surface, whereas the samples recovered at room temperature after thermal treatments leading to the formation of phases II and III, showed uniquely the typical diffraction patterns of I. The disappearing of I* is independent from the atmosphere in which the heating is performed.

The attention was therefore directed to the characterization of phases IV and V, and in particular concentrated on the samples utilized for the magnetic characterization. For each sample, several grains were investigated, to improve the statistical significance of the observations. The general picture offered by the several collected SAED patterns is

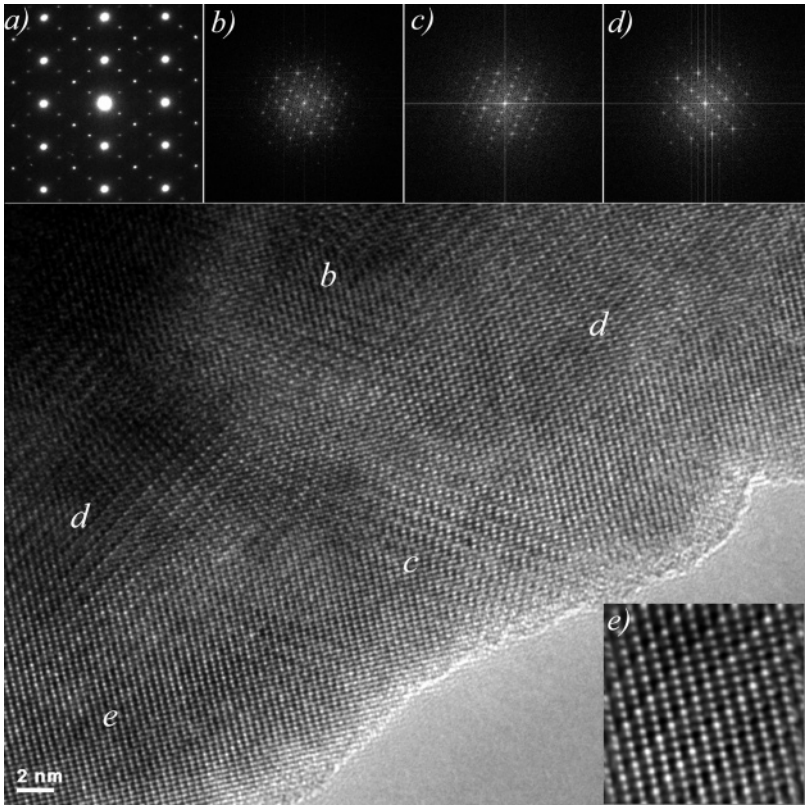

Figure 11. HREM image taken along $[101]_P$, showing the coexistence of modulation domains frequently observed in sample A: (a) experimental SAED pattern; (b−d) FFT of the selected area indicated by the same label; (e) enlargement of the HREM image of region with the corresponding label.

rather complex. On one side, the analysis is complicated by the pseudocubic nature of the structure, resulting in a strong similitude of the lattice parameters and in the occurrence of twinning on a scale, which is often smaller than the illuminated region (producing multidomain diffraction). On the other side, as pointed out by the magnetic characterization, the samples are never pure phases, so that patterns taken on different grains cannot be framed easily in common pictures.

Analysis of samples A and B confirmed the presence of phase I, previously evidenced by XRD and magnetic measurements. The observed SAED patterns can be grouped in two families. The first is characterized by the presence of commensurate satellite spots, not observed previously for $BiMnO_3$ polymorphs surviving at RT (I and I*) either compatible with ED patterns simulated on the basis of the I structure, and therefore are considered typical of structure IV. Some typical diffraction patterns, indexed in terms of the fundamental perovskite cell, are shown in Figure 10. The more characteristic feature is the existence of a commensurate 4-fold modulation along the $[110]_P$ direction of the fundamental perovskite reciprocal lattice. The second family shows on the contrary satellites quite similar to those observed for phase I, but in some cases, differences in the lattice parameters make ambiguous assignment of the pattern to the proper phase. An example is shown in Figure 11, where a multidomain experimental SAED pattern is compared with the corresponding HREM image and with the fast Fourier transform (FFT) of selected regions. The existence of two partially interpenetrated modulation domains is clearly revealed by the HREM image and its FFTs. On one side the FFT of single domain regions shows the typical satellites of phase I in similar zone axes, but this type of twinning, occurring frequently in sample A and giving rise to sharp satellites and fundamental spots (no doubling is detected in the experimental SAED), was never observed previously in I samples.

Due to these problems, the derivation of an unambiguous commensurate superstructure describing variant IV is not possible, at least starting from the SEAD patterns we collected, even if a large supercell with 4-fold perovskite parameters seems to be necessary (as for I*) to index all the satellite reflections. The suggestion, given by the XRD analysis, that IV would be a low-symmetry phase, was confirmed by SAED patterns. By an accurate selection of single-domain patterns, a reasonable setting of the fundamental cell was obtained by QED[23] as $a = 3.96$ Å, $b = 3.94$ Å, $c = 3.92$ Å, $\alpha = 90.3°$, $\beta = 89.7°$, and $\gamma = 90.8°$. Starting from these values and using a simple $BiMnO_3$ perovskite model just to provide a reasonable estimation of the diffraction intensities, we tried to refine the lattice parameters of IV by Rietveld analysis of the XRD diffraction pattern, obtaining a reasonable fitting of the convoluted diffraction profile with lattice parameters close to those derived from ($a = 3.951(1)$ Å, $b = 3.935(1)$ Å, $c = 3.908(1)$ Å, $\alpha = 90.25(2)°$, $\beta = 89.87(2)°$, $\gamma = 90.40(2)°$, and $V = 60.76(3)$ Å^3). On this basis the irreversible III−IV transition results in a further decrease of the cell volume, in agreement with the hypothesis of a phase oxidation realized through cationic deficiency instead of extra oxygen.

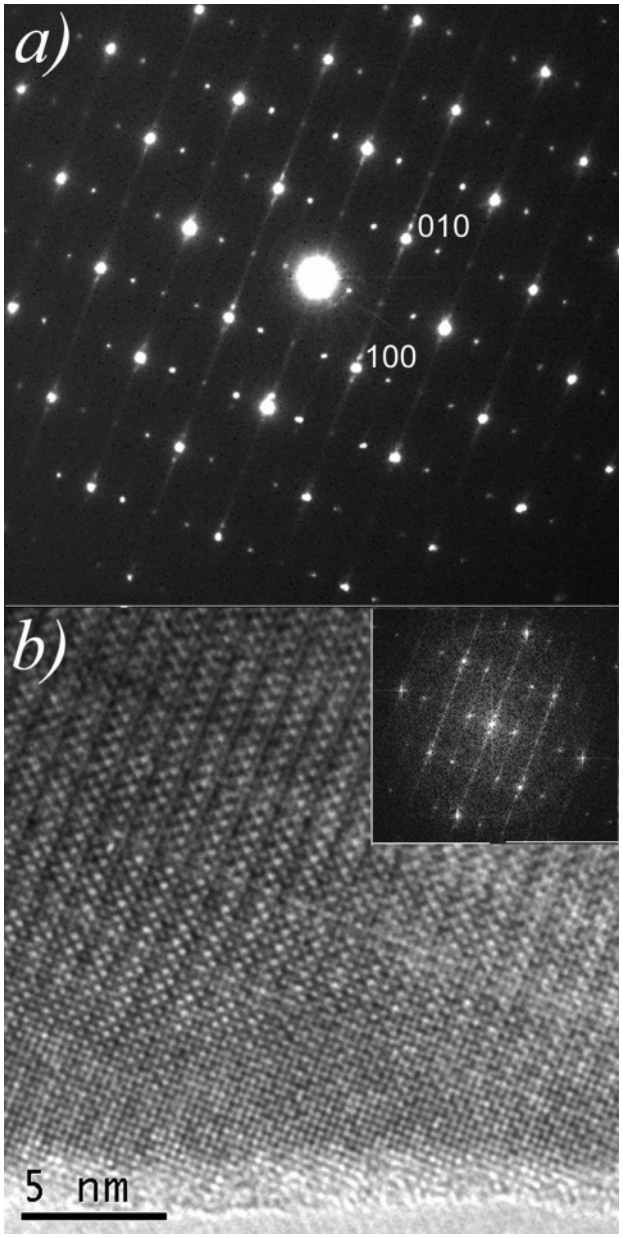

Figure 12. (a) $[001]_P$ SAED pattern taken on sample B, showing the simultaneous presence on commensurate and incommensurate modulation in the **a***__b__* plane of the reciprocal lattice; (b) HREM image of the corresponding area. The image FFT is shown in the inset.

TEM investigation on sample B pointed out an interesting evolution of the IV structure. In a few grains the commensurate 4-folding along $[110]_P$ was found to be coupled to a second modulation (Figure 12), running in the perpendicular direction $[\bar{1}10]_P$ and showing an incommensurate wave vector $\mathbf{q} = 0.095(-\mathbf{a}^* + \mathbf{b}^*)$. Successive analysis of samples C and D confirmed this modulation as the characteristic signature of the IV−V transition. However, by increasing the annealing time, the incommensurate modulation along the $[\bar{1}10]_P$ direction transforms into a diffuse streaking (Figure 13), indicating the degeneration of the periodic incommensurate modulation into a disordered stacking of different periodicities, probably connected with structural disorder introduced by local changes of the

(23) Belletti, D.; Calestani, G.; Migliori, A.; Gemmi, M. *Ultramicroscopy* **2000**, *81*, 57.

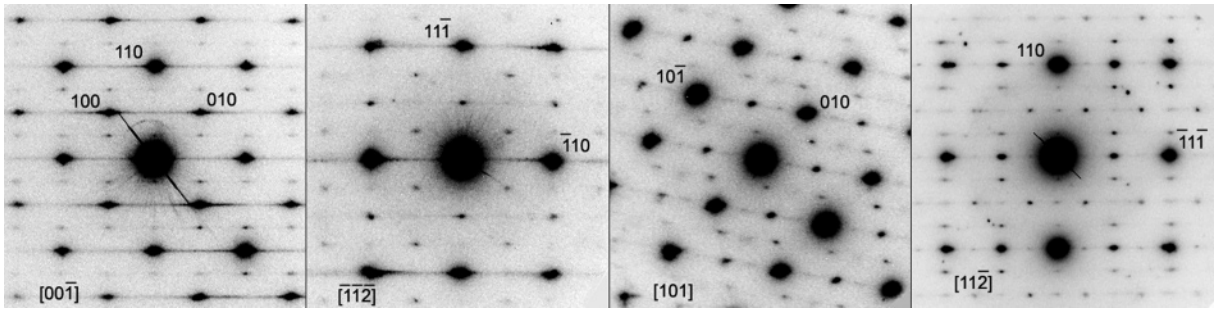

Figure 13. SAED patterns taken in different zone axes on the same grain of sample C showing the typical modulation feature of phase V.

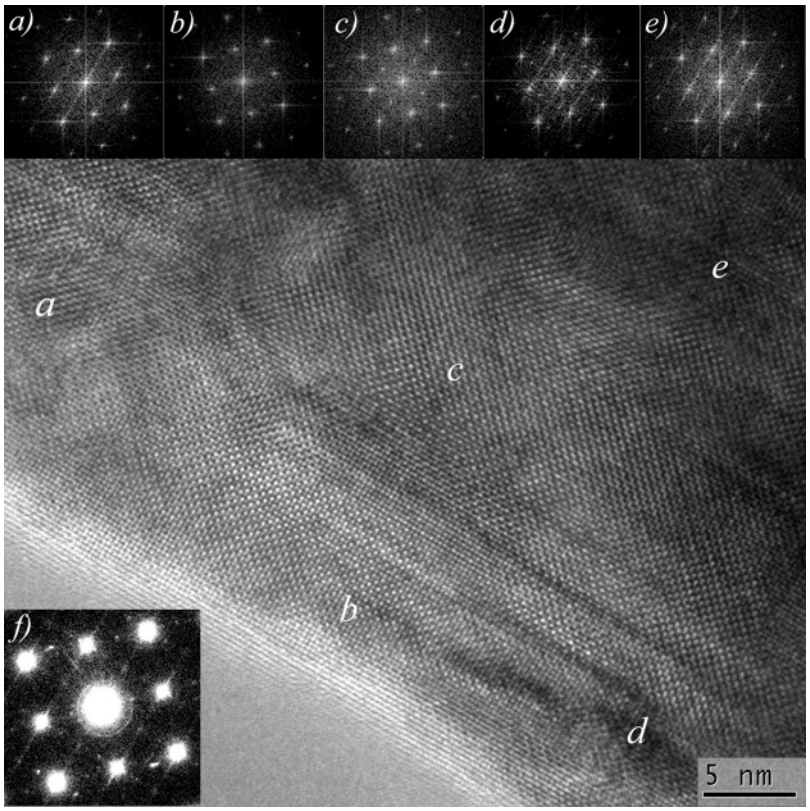

Figure 14. Short-range coexistence of nanosize domains in a HREM image taken along a fundamental perovskite axis on sample D. (a−e) FFT of selected area indicated by the same label; (f) experimental SAED pattern taken on a larger area resuming all the previous features joined to a diffuse streaking arising from additional twinning.

chemical composition. HREM images, taken in the fundamental $[001]_P$ zone axis pointed out the coexistence of very small domains, each one characterized by different modulation features in the fundamental (110) plane, as shown in Figure 14. Therefore, V could be considered a nonstoichiometric phase and the broadness of the magnetic transition could be related to compositional changes.

The appearing of the incommensurate modulation is related to an increase of the distortion of the fundamental perovskite cell, already revealed by XRD. By an accurate selection of single-domain patterns, a reasonable setting of the fundamental cell was obtained as $a = 3.95$ Å, $b = 3.93$ Å, $c = 3.87$ Å, $\alpha = 90.3°$, $\beta = 89.7°$, and $\gamma = 90.5°$. Starting from these values and using a simple $BiMnO_3$ perovskite model just to provide a reasonable estimation of the diffraction intensities, the lattice parameters of V were refined by Rietveld analysis of the XRD diffraction pattern, obtaining a reasonable fitting of the convoluted diffraction profile with lattice parameters close to those derived from ED ($a = 3.949(1)$ Å, $b = 3.922(1)$ Å, $c = 3.868(1)$ Å, $\alpha = 90.27(4)°$, $\beta = 89.89(5)°$, and $\gamma = 90.54(2)°$, and $V = 59.91(2)$ Å^3). By comparison with IV, V shows a reduced cell volume, confirming a progressive contraction of the structure by increasing the oxidation degree.

TEM results can be considered in good agreement with both magnetic and XRD characterization. On one side, the existence of two magnetic effects at about 70 and 50 K can be associated with characteristic structural features of these samples revealed by XRD and TEM. On the other side, HREM generally pointed out short-range twinning that can account for the very broad unresolved diffraction pattern.

Conclusions

The thermal evolution, depicted in Figure 15, of the metastable $BiMnO_3$, prepared at high pressure, was investigated in the temperature range of RT to 550 °C by HTXRD.

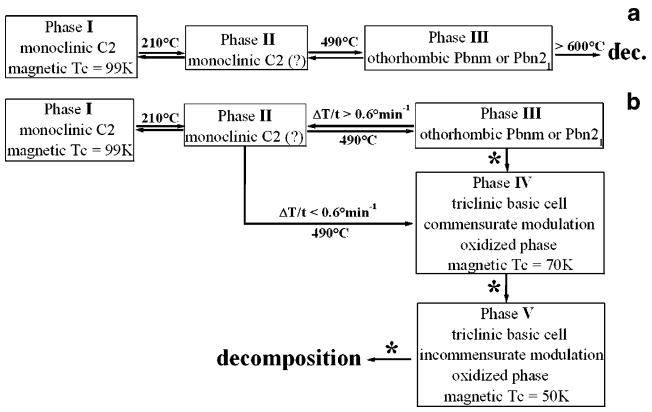

Figure 15. Schematic illustration of the thermal evolution of $BiMnO_3$ at ambient pressure in inert gas (a) and in air (b). The temperatures marked by stars, in general above 490 °C, are strongly dependent on heating rate and annealing time.

The results, coupled with TEM investigations (SAED and HREM) and magnetic measurements performed on the samples after different thermal treatments, pointed out the existence of different thermal pathways to the thermal decomposition of the phase and a complex picture of its polymorphisms, depending on the heating rate and atmosphere. According to previous literature, the as-prepared sample (mainly consisting of the monoclinic phase I) transforms reversibly to a second monoclinic phase (II) at 210 °C, whose further evolution leads to a tetragonal (according to Faqir et al.[20]) or to an orthorhombic (according to Kimura et al.[7]) phase. We found a reversible transition to the orthorhombic phase (III) at 490 °C, when II is heated in inert atmosphere. The same transition is observed in air, when the heating rate is kept sufficiently high ($\geq 0.6°$ min^{-1}). All the transitions involving polymorphs I−III are fast and reversible, suggesting a displacive character. The reversibility of the phase transitions agrees with the endothermic effect detected on heating by DSC. Being I at room conditions a metastable phase, all these transitions should be interpreted thermodynamically as transformations occurring in a metastability regime (from a metastable phase to another metastable phase). Even if the phases are characterized by a positive trend of the thermal expansion, the transitions occur, on heating, with a decrease in volume. Therefore, II and III are expected to be stabilized at lower temperatures by increasing pressure, in agreement with the observed increase of the I−II transition temperature to 380 °C, when operating in a vacuum.

From the structural point of view polymorph II shows, when compared with I, a slightly distorted cell and a similar diffraction symmetry (possible space groups from systematic absences are *C*2, *Cm*, or *C*2/*m*), so that a strong similarity could be hypothesized. On the other hand, the XRD pattern of the orthorhombic III modification shows analogies with $Bi_{1-x}Ca_xMnO_3$.[22] This probably induced Kimura et al.[7] to consider a centrosymmetric space group (*Pbnm*), postulating a paraelectric behavior of the phase. In reality, no direct evidence of a paraelectric region for $BiMnO_3$ was supplied in the literature until now, since dielectric measurements above 100−150 °C are hampered by the low resistivity of the specimens. Therefore, since the space group cannot be unambiguously defined by systematic absences (the noncentrosymmetric *Pbn*2_1 is also possible), only a careful refinement of the crystal structure could assign the correct space group. However it would require accurate neutron data, due to the low scattering contribution of oxygen atoms of the bismuth manganite in XRD.

When III is heated in an oxygen-containing atmosphere above the II−III transition temperature, a slow irreversible transition to a new variant IV takes place, with a kinetic depending on temperature, heating rate, and oxygen partial pressure. A II−IV direct transition is observed in air at 490 °C (II−III transition temperature), when a sufficiently slow heating rate ($\leq 0.5°$ min^{-1}) is applied. Increase of the annealing time in the same conditions produces a further structural variant V. The requirement of an oxygen-containing atmosphere induced us to consider IV and V as progressively oxidized phases containing Mn^{4+}, hypothesis supported by further experimental evidences. Consequently, IV and V cannot be strictly considered $BiMnO_3$ polymorphs, since they can be obtained through a chemical reaction involving a change of the chemical composition. However, they preserve a strong structural analogy with the $BiMnO_3$ phases, of which they can be considered compositional variants ($Bi_{1-x}MnO_3$). For both phases, our XRD analyses and TEM observations are consistent with a modulated structure based on a distorted fundamental triclinic perovskite. The modulation features range from commensurate in IV to incommensurate in V (often degenerated in a disordered aperiodic stacking). Both phases are ferromagnetic, with characteristic temperatures of 70 and 50 K, respectively, and with an effective moment that decreases with the increase of the Mn^{4+} content.

The existence of different magnetic phases in the complex $BiMnO_3$ system induces reconsideration of the recent literature, in particular concerning thin film preparation and characterization. It is quite interesting to note that the magnetic characterization of thin films, when reported, shows behaviors of the magnetization vs temperature curves that are often comparable with the ones we recorded on samples containing phases IV and V. For example, the one reported for thin films grown on $SrTiO_3$ substrate by pulsed laser deposition[12] is quite similar to the measurement we performed on sample A (IV contaminated by I). Sharan et al.[6] reported that the typical film stoichiometry, determined by Rutherford backscattering spectroscopy (RBS), is Bi-deficient, as it would be expected for an oxidized phase. Despite this, the films are quite promising, showing large third-order optical nonlinearities and giant electric-field-induced enhancement of the second harmonic response.[5,6] Thin films grown by the same technique on $LaAlO_3$ and Pt/TiO_2/SiO_2/Si substrates show a magnetic transition below 50 K,[14] in agreement with what we observed for V. However, nanosize bits of ferroelectric polarization can be written and read on these films by Kelvin force microscopy (KFM). In a very recent publication[24] the application of ultrathin films of $BiMnO_3$ as spin filters has been investigated. In such films

(24) Gajek, M.; Bibes, M.; Barthélémy, A.; Bouzehouane, K.; Fusil, S.; Valera, M.; Fontcuberta, J.; Fert, A. *Phys. Rev.* **2005**, *B72*, 020406 (R).

the magnetic properties (for instance the magnetic Curie temperature is suggested to be at about 40 K when the spin-filter effect vanishes) and the observed off stoichiometry of the phase present strong analogy with variant V. All these results indicate that the existence of multiferroism in the Bi−Mn−O system has been probably considered in a restrictive way, as confined in a specific structural modification, whereas its possible extension to the other magnetic perovskite-type manganites should be considered and verified.

Acknowledgment. We thank Dr. Guglielmina Gnappi (University of Parma) for thermal analyses and Dr. Simone Fabbrici (CNR-IMEM) for his collaboration.

CM051576W